Broadband absorption enhancement in hole-transport-layer-free perovskite solar cell by grating structure

Hamideh Talebi[1]*, Farzin Emami[1], and Esmat Rafiee[2]

1. Nano‑Optoelectronic Research Center, Electronic Department, Shiraz University of Technology, Shiraz, Iran

2. Department of Electrical Engineering, Faculty of Engineering, Alzahra University, Tehran, Iran

Recently, the hole transport layer-free planar perovskite solar cells (HTL-free PSCs) have attracted intense attention. However, the poor absorption of light in the wavelengths longer than 800 nm is an important challenge in all configurations of PSCs. In this study, the HTL-free PSC with a gold rectangular grating at back contact is proposed. In order to improve the performance of the solar cell, effects of grating dimensions and periodicity on the absorption of the active layer are numerically investigated. In the improved condition, an absorption enhancement of 25% in the range of 300—1 400 nm is obtained compared with the flat electrode-based structure. These improvements are attributed to the coupling of light to surface plasmon polariton (SPP) modes. Also, the electrical simulation results of the improved solar cell demonstrated short-circuit current density and power conversion efficiency of 27.72 mA/cm^2 and 18%, respectively.

Perovskite solar cells (PSCs) are promising approaches to high-performance photovoltaic[1]. There are of great interest due to their unique optical and electrical properties, long charge emission lengths, high charge mobility, low fabrication cost and simple synthesis methods[2]. However, one of the limitations of PSCs, which is poor light absorption in the near-infrared (NIR) region due to the relatively weak extinction of the perovskite absorber layer in this region, has received less attention[3]. However, only in a few recent studies, light management techniques based on nanoparticles (NPs) have been used to improve the light absorption in this region[4,5]. The radiative effects of local surface plasmon resonance (LSPR) supplied by the NPs including light scattering and near-field enhancement are responsible for the absorption increment[6]. Another light management structure that can enhance the light-harvesting efficiency is the grating structure[7]. The grating structures depending on their position in the cell can improve the device performance by increasing the length of the light path, coupling the incident light with propagated modes, or reducing light reflections[8].

It should be considered that in PSCs, the grating structures had been less considered. Recently, one or two-dimensional metallic grating nanostructures placed at the top of PSC[9], at the interface of the perovskite layer with holes transport layer[10-12], or the electron transport layer (ETL)[13-16] have been used to improve optical absorption. Also, the various patterned back contact structures have been utilized to increase optical field and optical absorption[17]. However, most studies have focused on non-plasmonic grating structures. In addition, the reported studies based on grating are limited to structures that include a charge transfer layer between perovskite and electrodes. Since plasmonic modes have a limited penetration depth[18], the absence of charge transfer layers leads to the full use of plasmonic effects in the absorber layer. Also, PSCs without a transport layer, such as hole transport layer-free PSC (HTL-free PSC), is one of the most efficient and appropriate configurations, which has better stability and lower process cost and temperature than other configurations[19]. Also, all research attentions have been focused on the absorption of the planner solar cells in the 300—800 nm wavelength ranges. So far, the PSC with the back plasmonic grating electrode that improves the light absorption in both visible and NIR bands has not yet been reported.

In the present study, a one-dimensional gold periodic grating on the back electrode of HTL-free planar PSC is used to improve the optical absorption in the NIR region. In the first step, by applying an analytical approach, PSC optical modeling is performed for calculating optical absorption and photo-generation rate. The effects of grating dimensions and periodicity on the absorption of the active layer are also investigated, leading to the improved structure. It should be noted that unlike most studies, the losses due to the absorption of gold grating are considered in all stages. After calculating the generation

* E-mail: h.talebi.1988@gmail.com

rate for the improved structure, photovoltaic characteristics of the improved proposed HTL-free PSCs are achieved by conducting the electrical analysis.

The suggested structure of HTL-free planar PSCs is depicted in Fig.1(a). The structure consists of glass (400 nm)/indium tin oxide (ITO) (60 nm)/TiO$_2$ (60 nm)/CH$_3$NH$_3$PbI$_3$ (400 nm)/Au (40 nm) with Au rectangular grating on the back contact. Thicknesses of different layers of solar cells have been chosen based on experimental studies[20,21]. In this structure, TiO$_2$ is employed as ETL to extract excited carriers in the CH$_3$NH$_3$PbI$_3$ layer. Since only two elements, Au and carbon are utilized as back electrodes in HTL-free PSCs, and Au is considered as the back electrode. ITO is utilizes as the transparent conductive oxide electrode. The diagram of the simulated unit cell with the back grating contact is shown in Fig.1(b). The height, width, and periodicity of the grating electrode are denoted with h, w, and p, respectively. The complex refractive indices of the layers are considered from the reported papers[5,22].
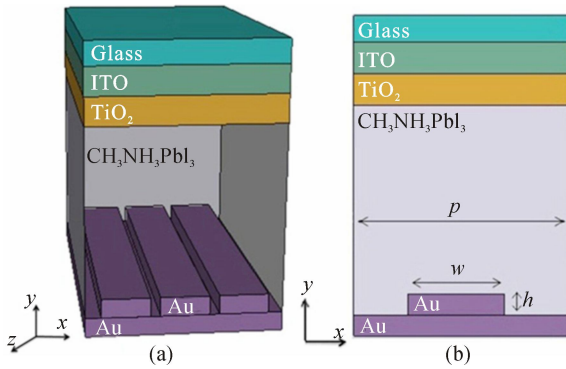
Fig.1 (a) 3D schematic of the proposed PSCs with rectangular grating back contact; (b) Diagram of the simulated unit cell with grating back contact

A two-step analysis is performed to obtain the solar cell parameters. First, the effect of the grating contact on the optical response of the solar cell is studied by using the finite-difference time-domain (FDTD) method. Three-dimensional structures that respond to arbitrary light polarization can often be extracted the same as the two-dimensional model with transverse magnetic (TM) polarization. For this reason, a two-dimensional simulation with TM polarization is considered in which the magnetic field has a component in the z-direction. A 1 000 W/m^2 plane wave at the normal angle is considered as incident light. The simulation wavelength range is considered from 300 nm to 1 400 nm. All simulations are carried out in a unit cell. The periodic boundary conditions are applied at the left and right unit cell, while perfectly matched layers are considered at the top and bottom of the unit cell. The high-density non-uniform mesh is applied in grating area.

A light absorption in the active layer is achieved according to[22]

$$A(\lambda) = \frac{\iint \frac{\pi c}{\lambda} \mathrm{Im}(\varepsilon_r) |E|^2 \, \mathrm{d}x \mathrm{d}y}{P_{in}}, \tag{1}$$

where λ, c, E, $\mathrm{Im}(\varepsilon_r)$, and P_{in} demonstrate the wavelength, the light speed in a vacuum, the electric field amplitude, the imaginary part of the dielectric permittivity of perovskite, applied field power, respectively. The grating electrode absorptivity is calculated using the same equation at the grating surfaces. This absorption is parasitic absorption and has no role in generation current. Therefore, by reducing the parasitic absorption from the total absorption of the perovskite layer, the net absorption of the active layer can be achieved. The net absorption spectrum (related to the active layer) is used in the following sections.

The short-circuit current (J_{SC}) can be obtained through integration of light absorption with solar radiation in the wavelength range of 300—1 400 nm[22]

$$J_{SC} = \frac{q}{hc} \int_{\lambda_1}^{\lambda_2} A(\lambda) \lambda I_{AM1.5}(\lambda) \mathrm{d}\lambda, \tag{2}$$

where h and q represent the electron charge, the Planck constant and the electron charge, respectively. Also the $I_{AM\,1.5}$ is the solar spectral irradiance intensity.

Considering the net absorption spectrum and that electron-hole pairs are created by absorbed photons, the optical generation rate $G_{opt}(\lambda)$ can be considered as[22]

$$G_{opt}(\lambda) = \frac{A(\lambda)}{\hbar\omega} = \frac{\varepsilon''(\lambda)|E|^2}{2\hbar}, \tag{3}$$

where $\hbar$ and ω stand for the reduced Planck constant and angular frequency of the applied light, respectively.

The current density-voltage (J-V) spectrum can be obtained by considering the generation rate as a source term in the electrical model. The photovoltaic parameters are achieved by calculating the coupled Poisson and continuity equations[22]

$$\frac{\mathrm{d}^2 V}{\mathrm{d}x^2} = \frac{q(p - n + N_D^+ - N_A^-)}{\varepsilon}, \tag{4}$$

$$\frac{\partial n}{\partial t} = \frac{1}{q} \frac{\partial J_n}{\partial x} + (G_n - R_n), \tag{5}$$

$$\frac{\partial p}{\partial t} = \frac{1}{q} \frac{\partial J_p}{\partial x} + (G_p - R_p), \tag{6}$$

where $J_n(J_p)$, $n(p)$, $N_A(N_D)$, V and R represent the electron (hole) current density, the electron (hole) and the acceptor (donor) concentrations, the electrostatic potential and recombination rate, respectively. The J-V characteristic can be calculated according to the following equations[22]

$$J_n = q\mu_n nE + qD_n \nabla n, \tag{7}$$

$$J_p = q\mu_p pE - qD_p \nabla p, \tag{8}$$

where $\mu_n(\mu_p)$, and $D_n(D_p)$ indicate the electron (hole) mobility, and the electron (hole) diffusion coefficient, respectively. The diffusion coefficient which depends on the mobility and carrier lifetime can be obtained by Einstein relationship[22]

$$D_{(n,p)} = \sqrt{\mu_{(n,p)} \frac{KT}{q} \tau_{(n,p)}}, \qquad (9)$$

where K and T indicate electron (hole) lifetime, Boltzmann constant, and temperature. The parameters used in the simulations are presented in Tab.1.

Tab.1 Physical parameters of the layers used in the simulations

Parameters	Compact TiO$_2$	CH$_3$NH$_3$PbI$_3$
Dielectric permittivity	10[24]	10[24]
Electron mobility (cm^2/Vs)	100[24]	1.00[24]
Hole mobility (cm^2/Vs)	25[24]	1.0[24]
Acceptor concentration (1/cm^3)	0	$1.0 \times 10^{14[24]}$
Donor concentration (1/cm^3)	$1.0 \times 10^{17[24]}$	0
Band gap (eV)	3.26[24]	1.5[24]
CB (1/cm^3)	$2.0 \times 10^{17[24]}$	$2.75 \times 10^{18[24]}$
VB DOS (1/cm^3)	$6.0 \times 10^{17[24]}$	3.9[24]
Affinity (eV)	4.2[24]	3.9[24]

The effects of Au grating electrode on the absorption of the active layer are investigated in this part. A solar cell with a flat gold electrode is considered as a reference device in all stages. The three absorption curves discussed in the proposed device, including total, parasitic and net absorption are shown in Fig.2. Fig.2(a) shows the parasitic absorption of the grating structure, the total and net absorption of the perovskite layer in the proposed solar cells. Absorption of perovskite in the solar cell with flat electrode is also plotted in the same figure in order to conduct the comparison. It is also clear that the reference device shows strong absorption in the ranges of ultraviolet and visible while showing weak absorption in the NIR region due to the small extinction coefficient. The net absorption of the perovskite layer in the proposed solar cell shows a good absorption improvement in the wavelength ranges from 620 nm to 780 nm. A broadband absorption enhancement is also observed at the wavelength 800—1 200 nm. In addition, there is not much difference in perovskite layer absorption in the proposed and reference solar cells at wavelengths above 1 200 nm. Also, the absorption of the grating structure demonstrates that the parasitic absorption is high in long wavelengths. As a result, if the loss is not considered in the current relation, the current of the solar cell can be incorrectly increased.

Moreover, the net absorption curves of the active layer with the periodicity of 120 nm, 300 nm, and 600 nm are shown in Fig.2(b). The height and width of the grating structure are considered as 30 nm and 100 nm, respectively. As shown in Fig.2(b), in the solar cell with a grating periodicity of 120 nm, significant absorption improvement is seen at wavelengths less than 1 200 nm. Whereas, in the higher period, a lower absorption enhancement is achieved in the wavelength ranges from 800 nm to 1 200 nm, and no absorption is observed in

longer wavelengths. Nevertheless, absorption is improved in structures with higher periods relative to the reference structure in the visible region.
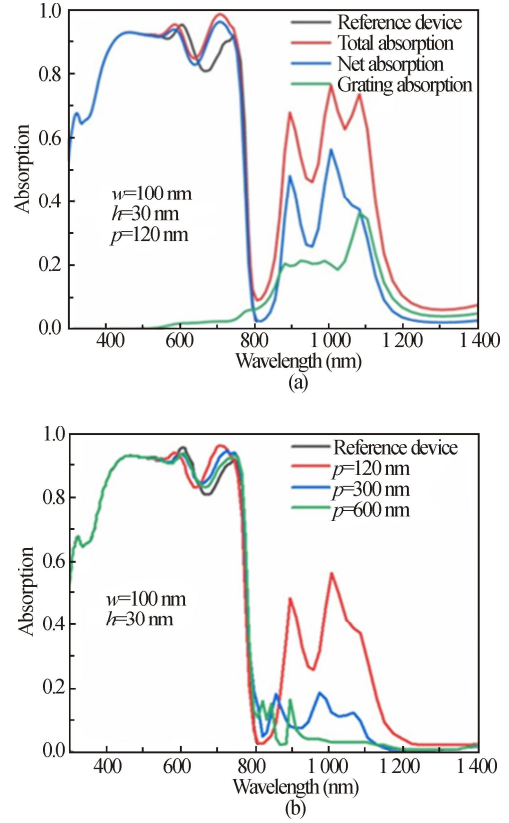
Fig.2 (a) The net and parasitic absorption spectra of the perovskite in devices with flat back contact and grating structure; (b) Proposed PSCs (*h*=30 nm, *w*= 100 nm) absorption spectra with structure period of 120 nm, 300 nm, and 600 nm

To understand the mechanism of absorption increment by adding a grating structure to the solar cell, the electric field distribution in the perovskite layer is investigated. The electric field distributions in the perovskite layer and Au electrode for reference and proposed solar cell are shown in Fig.3 at three wavelengths of 656 nm, 880 nm, and 1 123 nm. The height and width of the grating structure are considered as 30 nm, and 100 nm, respectively. The periodicity is set in two values of 120 nm and 600 nm. Field profile and intensity are the same in the device with various periodicities and reference devices at a wavelength of 656 nm (Fig.3(a), (d) and (g)). Since perovskite has an intense absorption coefficient in the wavelength region lower than 656 nm, the light is absorbed on the perovskite surface. So the incident wave does not reach the depth of the active layer, and the grating back contact does not play a role in improving the absorption in this area. While due to poor absorption of the perovskite layer in the wavelength region longer than 656 nm, incident wave penetrates to the depth of perovskite in these areas. On the other hand, the refractive

index of perovskite is higher than other materials, and the photoactive layer operates relatively like a Fabry-Pérot cavity with partial mirrors created by Fresnel reflection at its interface. Therefore, the electric field profile shows the standing wave formation in the perovskite layer at longer wavelengths in reference solar cells (Fig.3(b) and (c)). But, different patterns in the electric field distribution are obtained at longer wavelengths for different periodicities of the grating. As shown in Fig.3(e) and (f), strong field enhancement is obtained at the perovskite/gold interface in structures with periods of 120 nm at longer wavelengths. This strong field corresponds to surface plasmon polariton (SPP) mode of grating structure. Whereas, in a structure with a periodicity of 600 nm, the strong electric field is seen inside the active layer at the wavelengths of 880 nm, which is attributed to the excitation of second-order waveguide modes, as shown in Fig.3(h). In addition, weak plasmonic modes are excited at wavelengths of 1 123 nm (Fig.3(i)). Therefore, SPP and waveguide modes are dominant in the structures with lower and higher periods of grating, respectively.
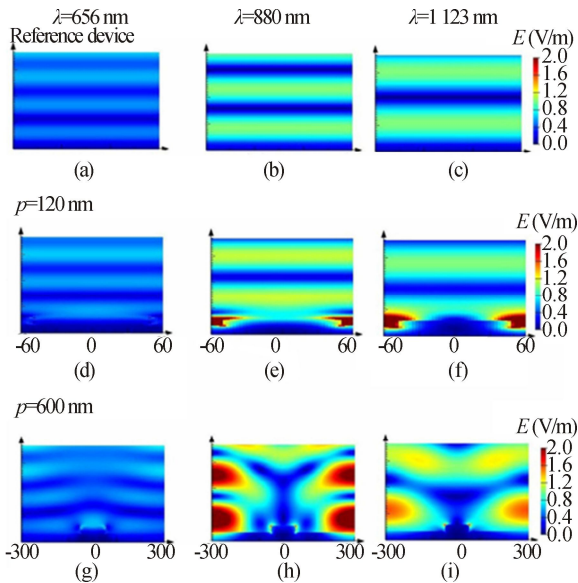
Fig.3 Electric field profiles at wavelengths of 656 nm, 880 nm, and 1 123 nm for (a—c) reference device, and (d—i) the proposed PSCs with different periods

The change in the distribution of modes with the change in the periodicity of the structure is due to the changes in the effective index of the structure. Interaction of the incident light with this mode and its field distributions leads to absorption improvement, because the absorptivity mainly depends on the electric field intensity. The effect of each mode on the performance of the solar cell is investigated by studying the absorption curve. As a result, according to the absorption spectrum (Fig.2(b)) and distribution of the field in the wavelengths corresponding to the absorption peak, it can be concluded that plasmonic modes have a more significant effect on im-

proving the absorption rate than the guided modes.

To maximize the light-harvesting of PSC and fully exploit the effects of grating back contact, the effects of grating height, width, and periodicity on the performance of the grating structures are also studied. First, the impacts of the grating height and width are investigated for a period of 100 nm. The density of the maximum achievable optical current, called short-circuit current density, is selected as the base comparing factor. For this purpose, the contour plot of J_{SC} is plotted as a function of the grating width and height, as seen in Fig.4(a). The J_{SC} is almost constant and has a value of 25 mA/cm^2 for different geometric parameters (heights of 10—60 nm and widths of 50—90 nm). However, the maximum J_{SC} of 27.72 mA/cm^2 is obtained at the width and height of 75 nm and 30 nm, respectively. In addition, it must be mentioned that J_{SC} of the reference device is 22.06 mA/cm^2. In some grating geometries, the current of the proposed PSC is less than the reference device current due to the parasitic absorption losses of Au grating which have been considered in the calculations.

Next, the effect of the grating structure periodicity and the width ratio (i.e. w/p) on absorption is examined when the grating height is adjusted at 30 nm. As shown in Fig.4(b), currents up to 24.60 mA/cm^2 are achieved at different values of the period and the width ratio. However, the highest short-circuit current of 27.72 mA/cm^2 is obtained for structures with a periodicity of 100 nm and a width ratio of 0.75. Therefore, for the proposed solar cell, the improved parameters for the height, width, and periodicity of the grating are considered as 30 nm, 75 nm, and 100 nm, respectively.

The generation rate is shown as a function of the depth of the perovskite layer in the cell at the coordinate point x=38 nm in Fig.5(a). The generation rate at the upper part of the perovskite layer in solar cell with flat electrode and grating electrode is similar. Also, the maximum charge carrier generation rate in the reference structure, similar to the research, is located at the upper part of the perovskite. While in the proposed solar cell, the maximum rate is observed in the areas around the grating. In fact, in the vicinity of the grating structure, generation rate increases by 1 000× compared to the reference structure. The total carrier generation rates are obtained in the orders of and for the reference and the proposed structure, respectively.

The J-V characteristics of the improved and reference devices are calculated as shown in Fig.5(b). As seen, the reference device presents a J_{SC} of 22.06 mA/cm^2. The photocurrent significantly increases and reaches 27.72 mA/cm^2 by adding a grating structure on the back electrode. Also, an open-circuit voltage (V_{OC}) of 0.97 V is obtained for the improved proposed device, which is higher than that of the planar structure with a value of 0.92 V. Moreover, achievements exhibit a 37% improvement of the proposed device regarding power conversion efficiency (PCE) comparison with the reference device. PCE value increases from 13.13% in the reference cell to 18.0% in

the proposed PSC with an improved grating electrode. The results demonstrate the fill factor (*FF*) of 0.64 and 0.67 for the reference device and the improved device, respectively. The photovoltaic performances are also listed in Tab.2.

(a)

(b)
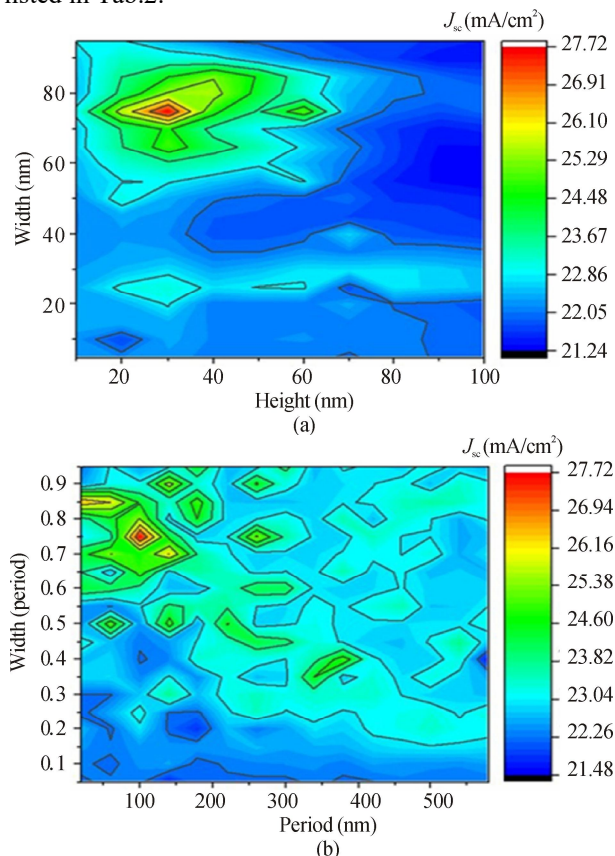
Fig.4 Contour plot of short-circuit current density as a function of (a) Au grating width and height for a period of 100 nm, and (b) Au grating period and width ratio for the grating height of 30 nm

In this article, HTL-free planar PSC with periodic Au grating back electrode had been proposed and analyzed. The results showed that these structures were suitable for enhancing light absorption in the NIR region and, at the same time, had maintained good performance in the visible region. These enhancements are attributed to the coupling of the incident light with SPP modes at the

(a)

(b)
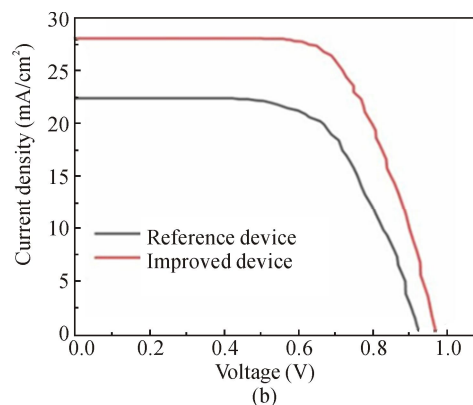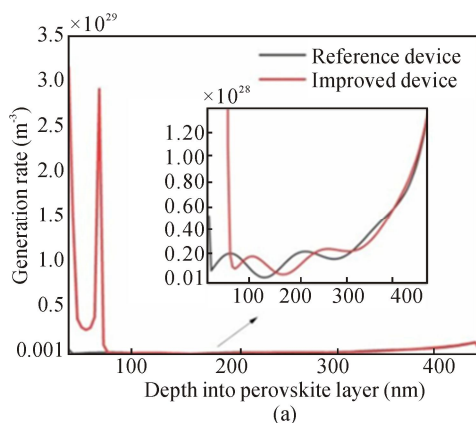
Fig.5 (a) The generation rate of electron-hole pairs in a perovskite layer as a function of distance into the PSCs; (b) *J-V* characteristics of pristine PSC and the improved proposed PSC

Tab.2 Photovoltaic performance of the PSCs

Device	J_{SC} (mA/cm^2)	V_{OC} (V)	*FF* (%)	*PCE* (%)
Reference device	22.06	0.92	0.64	13.13
Improved proposed device	27.72	0.97	0.67	18.00

perovskite/grating interface. The effects of grating parameters on the optical performance of the solar cell were also investigated, and the improved parameters were calculated. The improved height, width, and periodicity of the grating structure were obtained as 30 nm, 75 nm, and 100 nm, respectively. Absorption losses in the grating structure were calculated and taken into account in all steps. In the improved device, photocurrent density of 27.72 mA/cm^2 and efficiency of 18% were achieved, showing a 37% increment in efficiency compared to the reference structure.

Ethics declarations

Conflicts of interest

The authors declare no conflict of interest.

References

[1]   PARK N G. Perovskite solar cells：an emerging photovoltaic technology[J]. Materials today, 2015, 18(2)：65-72.

[2]   ZHU H, ZHAO Z, CAO H, et al. Determination of bandgaps of photoactive materials in perovskite solar cells at high temperatures by in-situ temperature-dependent resistance measurement[J]. Optoelectronics letters, 2016, 12：337-339.

[3]   LÖPER P, STUCKELBERGER M, NIESEN B, et al. Complex refractive index spectra of CH$_3$NH$_3$PbI$_3$ perovskite thin films determined by spectroscopic ellipsometry and spectrophotometry[J]. Journal

of physical chemistry letters, 2015, 6(1)：66-71.

[4]   YUE L, YAN B, ATTRIDGE M, et al. Light absorption in perovskite solar cell：fundamentals and plasmonic enhancement of infrared band absorption[J]. Solar energy, 2016, 124：143-152.

[5]   TALEBI H, EMAMI F. Design of ultrathin hole-transport-layer-free perovskite solar cell with near-infrared absorption enhancement using Ag NPs[J]. Optics communications, 2020, 520：128553.

[6]   ALHARBI R, IRANNEJAD M, YAVUZ M. Gold-graphene core-shell nanostructure surface plasmon sensors[J]. Plasmonics, 2017, 12：783-794.

[7]   ELEWA S, YOUSIF B, ABO-ELSOUD M. Efficiency enhancement of intermediate band solar cell using front surface pyramid grating[J]. Optical and quantum electronics, 2021, 53(7)：1-18.

[8]   SALEHI M R, SHAHRAKI M. Circuit modeling of waveguide grating nanostructures in ultrathin solar cells[J]. IEEE transactions on nanotechnology, 2017, 16(4)：616-623.

[9]   ELEWA S, YOUSIF B, ABO-ELSOUD M. Improving efficiency of perovskite solar cell using optimized front surface nanospheres grating[J]. Applied physics A, 2021, 127：1-14.

[10]   SCHMAGER R, HOSSAIN I M, SCHACKMAR F, et al. Light coupling to quasi-guided modes in nanoimprinted perovskite solar cells[J]. Solar energy materials and solar cells, 2019, 201：110080.

[11]   WANG Y, WANG P, ZHOU X, et al. Diffraction-grated perovskite induced highly efficient solar cells through nanophotonic light trapping[J]. Advanced energy materials, 2018, 8(12)：1702960.

[12]   ZHANG H, FAN J, ZHANG J. Near-infrared absorption enhancement for perovskite solar cells via the rear grating design[J]. Optical and quantum electronics, 2020, 52：1-8.

[13]   DENG K, LIU Z, WANG M, et al. Nanoimprinted grating-embedded perovskite solar cells with improved light management[J]. Advanced functional materials, 2019, 29(19)：1900830.

[14]   SCHMAGER R, GOMARD G, RICHARDS B S, et al. Nanophotonic perovskite layers for enhanced current generation and mitigation of lead in perovskite solar cells[J]. Solar energy materials and solar cells, 2019, 192：65-71.

[15]   CAO F, WANG M, SUN H, et al. Ordered array structures for efficient perovskite solar cells[J]. Engineering reports, 2020, 2(11)：e12319.

[16]   ZHANG Y, LIU H, MIAO Y, et al. High absorptivity of perovskite solar cell enhanced by metal grating[J]. Optoelectronics letters, 2022, 18：658-661.

[17]   ABDELRAOUF O A M, SHAKER A, ALLAM N K. Front dielectric and back plasmonic wire grating for efficient light trapping in perovskite solar cells[J]. Optical materials, 2018, 86：311-317.

[18]   HUANG Y, WU Y, XU X, et al. Nano Ag-enhanced photoelectric conversion efficiency in all-inorganic, hole-transporting-layer-free $CsPbIBr_2$ perovskite solar cells[J]. Chinese physics B, 2022, 31：128802.

[19]   CHU Q Q, SUN Z, DING B, et al Greatly enhanced power conversion efficiency of hole-transport-layer-free perovskite solar cell via coherent interfaces of perovskite and carbon layers[J]. Nano energy, 2020, 77：105110.

[20]   QIN P, TANAKA S, ITO S, et al. Inorganic hole conductor-based lead halide perovskite solar cells with 12.4% conversion efficiency[J]. Nature communications, 2014, 5：3834.

[21]   GRENEVELD B, NAJAFI M, STEENSMA B, et al. Improved efficiency of NiO_x-based p-i-n perovskite solar cells by using PTEG-1 as electron transport layer[J]. APL materials, 2017, 5：076103.

[22]   MOULE A J, SNAITH H J, KAISER M, et al. Optical description of solid-state dye-sensitized solar cells. I. Measurement of layer optical properties[J]. Journal of applied physics, 2009, 106(7)：073111.

[23]   GRAY J L. The physics of the solar cell[M]//Handbook of photovoltaic science and engineering. New York：John Wiley & Sons, Ltd, 2003：61-112.

[24]   HOSSAIN M I, ALHARBI F H, TABET N. Copper oxide as inorganic hole transport material for lead halide perovskite based solar cells[J]. Solar energy, 2015, 120：370-380.